Machine learning-based method to support TSO-DSO adaptive coordination with active power management for instability prevention

Chrysostomou, Demetris; Torres, José Luis Rueda; Cremer, Jochen Lorenz

DOI
10.1016/j.ijepes.2025.111353

Publication date
2025

Document Version
Final published version

Published in
International Journal of Electrical Power and Energy Systems

Electrical Power and Energy Systems 173 (2025) 111353

Contents lists available at ScienceDirect

International Journal of Electrical Power and Energy Systems

journal homepage: www.elsevier.com/locate/ijepes

Machine learning-based method to support TSO-DSO adaptive coordination with active power management for instability prevention

Demetris Chrysostomou *, José Luis Rueda Torres, Jochen Lorenz Cremer

Department of Electrical Sustainable Energy, Delft University of Technology, Delft, The Netherlands

ARTICLE INFO

Keywords:
TSO-DSO coordination
Machine learning
Stability
Aggregated distribution system dynamics

ABSTRACT

Coordination between power system operators can improve the power system stability and effectively deploy resources in distribution systems (DS). The research work of this paper provides a coordination method to mitigate the impact of dynamic events on transmission systems (TS). The proposed method uses a machine learning (ML)-based model to estimate the collective dynamic response of DS under varying TS dynamic properties, DS operating conditions, and share of inverter base resources (IBRs). In addition, the ML-based model enables TS operators (TSOs) to provide feedback to DS operators (DSOs) for controlling the IBRs' active power output to prevent post-fault instabilities. The proposed TSO-DSO coordination method includes a risk-based active power setpoint optimizer for instability prevention. The proposed method uses existing measurement and IBR control platforms available in DS and estimates the post-fault DS dynamic response considering IBR active power control actions. Case studies on synthetic models of TS and DS covering the Zeeland province in The Netherlands illustrate the application of the proposed coordination and the instability risk mitigation when optimizing IBR setpoints.

1. Introduction

Inverter-based resources (IBRs) in distribution systems (DSs) affect the overall power system dynamic stability. DS IBRs operating in grid-forming (GFM) mode can support the dynamic stability of transmission systems (TSs) that suffer from low inertia. TS operators (TSOs) need to anticipate and evaluate the impact of controlling DS IBRs on system stability as IBRs in DSs replace TS resources. However, including active components and IBRs in DSs makes modeling, maintaining, and co-simulating TSs and DSs challenging [1].

Coordination between TSOs and distribution system operators (DSOs) is a topic of increasing interest [2–4]. As distributed energy resources (DER) flexibility becomes necessary, TSOs and DSOs must coordinate to avoid causing issues to one another [4]. Existing TSO-DSO coordination methods differ in the central entity and data exchange requirements [2]. Market-based TSO-DSO coordination differs by multiple elements [5]. DSO-centric coordination allows low data exchange between TSOs and DSOs using flexibility areas [6,7]. However, flexibility areas evaluate and estimate the available flexibility through steady-state simulations. Evaluating the flexibility for dynamic stability is underrepresented in TSO-DSO coordination methods.

TSOs must ensure their system's security, withstanding imminent contingencies without service interruptions [8,9]. The typical industry practice is deterministic, where all probable contingencies are treated with equal risk [9]. However, risk-based security assessment becomes more applicable as the contingency probability, risks, and consequences differ [8,9]. Probabilistic approaches can consider the contingency likelihood, probability, and consequences of instability [8]. The proposed coordination helps TSOs assess the risks and costs of probable contingencies compared to flexibility costs.

Different share between grid-following (GFL) and GFM inverters impacts the dynamic response of DSs [10]. GFM inverters improve the dynamic performance of power systems with enhanced response to load [11] and fault [10] events. However, GFM inverters have stability issues after faults due to current saturation [11–13]. Thus, controlling the DS GFM IBRs setpoints can enable TSOs to evaluate and, if possible, prevent post-disturbance instabilities, such as current saturation. Different TS inertia alters the response of the DS [14,15], and the system inertia is highly variable [15,16]. Methods for DS aggregated dynamic response representation (ADRR) aim to support dynamic studies for TSOs and DSOs by alleviating the DS modeling and simulating complexity. Existing ADRR approaches do not support controlling DS GFM IBR outputs and typically consider fixed TS dynamic properties throughout the ADRR development. Considering TSs with fixed, high inertia in ADRR modeling does not accurately represent the DS response for TSOs to assess the impact of controlling GFM IBR. Thus,

* Corresponding author.
E-mail address: D.Chrysostomou@tudelft.nl (D. Chrysostomou).

https://doi.org/10.1016/j.ijepes.2025.111353
Received 2 August 2025; Received in revised form 11 October 2025; Accepted 3 November 2025
Available online 19 November 2025

DS ADRR models should account for the variable TS dynamic properties and support controlling the DS GFM IBR setpoints.

This research proposes a TSO-DSO coordination method that enables TSOs to evaluate and request flexibility from GFM IBRs for dynamic support. The proposed method applies in close to real-time operation, to prevent dynamic instability from possible dynamic events. Flexibility corresponds to the DS resources whose operation can be altered by TSOs or DSOs to support system operation [17]. A DS ADRR is a key component in enabling this coordination, accounting for the variable TS dynamic properties, types of IBRs, and IBR setpoints. The proposed TSO-DSO coordination requires measurements currently available to system operators, identifies the GFM IBR setpoints minimizing instability risks, and includes a classifier identifying extreme instabilities.

DS ADRR approaches mainly use system identification approaches that rely on measured or simulated data [1,18]. The scarcity of data with large disturbances limits the potential for measurement-based ADRR models. System identification-based ADRR approaches can diversify to black box and grey box. Black box approaches use data to fit a model of an unknown, typically machine learning (ML)-based structure [19,20]. Grey box approaches assume a DS equivalent structure, e.g., a load, a synchronous, and a static generator, and use data to fit the structure's parameters [18,21]. Grey box models are easier to integrate with software for dynamic simulations. However, the grey box modeling selection of a specific system structure and parameters can impair the model representation for variable operating conditions. To allow representing various operating conditions, [22,23] provide different ADRR model parameters for different operating condition clusters. With increased diversity in IBRs and DERs in DSs, grey box approaches require more complex structures with several components [24,25], whereas ADRR models should ease the DS modeling and simulation complexity. Applying a grey box approach can be challenging for a ring system topology [25], and including external variables in grey box model structures can be challenging in mapping the external variables and structure components. Black box methods do not have these restrictions in operating conditions, IBR diversity, external variables, or system topology. As ML algorithms become more prominent, integrating ML models into dynamic simulation software becomes anticipated. ML-based ADRR models explored long-short-term memory (LSTM) recurrent neural networks (RNNs) [19], Gaussian process models [20], and artificial neural networks [26]. RNNs are developed for sequential data but cannot effectively include static features. [20] included static features with repeated power outputs and voltage inputs. The proposed black box approach utilizes RNNs but also considers static features for the initial operating conditions, IBR share, and TS inertia.

DS models used in ADRR approaches typically assume knowledge of the IBR types, as GFL [1,23]. However, GFM inverters become increasingly used. To account for differences in DS generation types, [23] model considers the mixture of synchronous and asynchronous generation but assumes asynchronous DER. [27] modeled GFM and GFL IBR types and used the DS IBRs and synchronous generator inertia to provide an ADRR model with a more accurate response. [27] assumed the DSOs know detailed characteristics of the IBRs, e.g., the inertia, droop, and damping constants, and a high TS inertia. [25] modeled GFM IBRs but also assumed known IBR characteristics and developed a complex ADRR model structure with one branch for each GFM inverter counteracting the ADRR appeal for DS model simplification. This research represents IBRs with GFL and GFM types and estimates these types using measurements without assuming detailed IBR parameter knowledge.

Preventive dynamic security assessment studies require dynamic models of the underlying systems to identify remedial actions [28]. These security assessment studies consider equally credible contingencies [29] or include contingency probabilities for instability risks [8]. These studies typically focus on TS operating conditions to minimize instability risks. The proposed method focuses on controlling DS IBRs and the impact of DS IBR dynamics that preventive dynamic security assessment studies mainly exclude.

This paper proposes a TSO-DSO coordination method where TSOs can use the ADRR model to select and evaluate flexibility setpoints for the IBRs. Therefore, the main contributions are:

1. Developing a TSO-DSO coordination method for dynamic stability based on the estimation of the aggregated dynamic response of DS using measurements available to system operators.
2. Extension of the method to also include an algorithm for risk-based evaluation and selection of TSO actions to prevent instability.
3. Proposing an approach representing the aggregated DS dynamic response accounting for variable dynamic system properties, the aggregated power output, and the type of primary control of IBRs, combining sequential and non-sequential features.

Case studies are performed on the synthetic system model of the Zeeland region in the Netherlands. The case studies showcase the active power setpoint optimizer, and ADRR model performance with regression and high instability classification. The following subsections are Section 2 TSO-DSO coordination; the proposed coordination approach and key components, Section 3 DS aggregated dynamic response representation for variable TS dynamic properties and IBR share; the proposed ADRR model structure, Section 4 case studies; the case studies, and Section 5 conclusion.

2. TSO-DSO coordination

As the share of DERs increases, IBR flexibility can help TSOs achieve operational stability. Assessing IBR flexibility for dynamic events is challenging for TSOs as:

1. TSOs would need real-time information on the available flexibility in DSs from each IBR type,
2. TSOs would need models to consider the post-disturbance dynamic response of interconnected DSs,
3. TSOs would need functionality to select DS IBR setpoints to improve the TS dynamic stability.

To mitigate these challenges, this paper introduces the coordination illustrated in Fig. 1. The ADRR is developed by the DSO and used by the TSO. In operation, the DSO applies the IBR classifier algorithm to inform the ADRR model about the real-time DS operating condition. The TSO uses the operating condition to evaluate the stability of the post-fault system. If the ADRR detects instability, the GFM IBR active power setpoint optimizer identifies the risk-minimizing setpoint for the GFM IBRs and informs the DSO. The DSO validates that the requests respect DS network constraints and sends the validated requests to the IBRs through real-time interface (RTI). If TSO requests are invalid for the constraints of the DS network, the TSO is informed to explore an alternative risk mitigation without altering IBR setpoints.

The proposed coordination utilizes and extends the RTI application, which mandates the participation of large DER and considers markets out of scope [30]. Nevertheless, characterizations in [5] on market-based TSO-DSO coordination can clarify the proposed coordination characteristics. Namely, the proposed approach considers a decentralized optimization. The TSO optimizes the setpoints for stability, the DSO optimizes setpoints for congestion management (existing RTI modality), and evaluates the TSO's setpoints for feasibility. The DERs whose setpoints are used are reimbursed with a uniform pay. The grid representation requires comprehensive grid data for the TSOs (transmission network and DS ADRR). Market participation of DERs does not impact the proposed coordination, as the ADRR features include the measured DER setpoints, which may have been altered due to market agreements. However, a real-time TSO or DSO setpoint can be applied on top of these agreements for grid security.

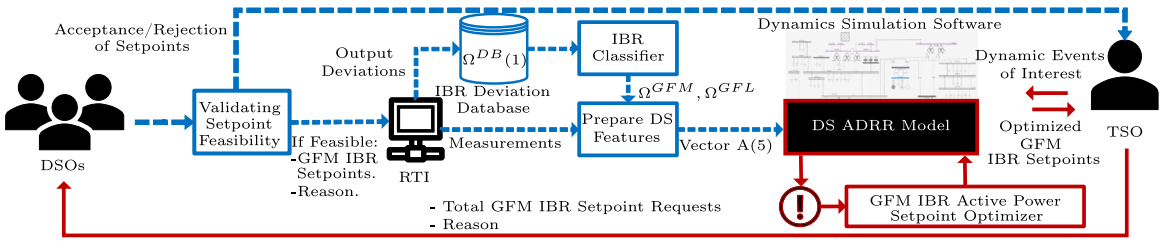

Fig. 1. Overview of the proposed TSO-DSO coordination with DSO-operated actions (⇢) and TSO-operated actions (→).

2.1. Estimating the real-time IBR outputs in DSs

DSOs have limited measurements in DSs [31]. This section describes how the proposed coordination considers the available measurements through the existing Dutch RTI technical framework to estimate the real-time IBR outputs in DSs. In 2020, Dutch DSOs and the TSO developed RTI to improve real-time communication between large DERs and DSOs, TSOs [30]. Through RTI, DERs with capacity 1–50 [MW], connected to the medium voltage, are required to measure and exchange information with the DSOs about the active power, reactive power, phase voltages, and phase currents. RTI measurements can have intervals of less than 60 [s]. Using RTI, the DSOs and TSO can request new power setpoints from DER to ensure their system's stability. The DSOs and TSO must include the reason for the requests.

The proposed coordination creates a database of IBR output deviations provided by RTI for DSOs to classify each IBR as GFM or GFL. These deviations are load change disturbances that occur continually [9], i.e., a sudden load consumption change. The database includes the wind speed deviation as uncertainty caused by variable weather conditions. These wind deviation values are attainable from weather radars. Set Ω^{DB} characterizes the database as:

$$\Omega^{DB} = \{(\Delta v_{jl}, \Delta i_{jl}, \Delta P_{jl}, \Delta Q_{jl}, \sigma_{jl}) | j \in \Omega^{DER}, l \in \Omega^{\Phi}\}, \tag{1}$$

where Ω^{DER} is the set of DER providing measurements through RTI, and Ω^{Φ} is the set of load disturbances. $\Delta v_{jl}, \Delta i_{jl}, \Delta P_{jl}, \Delta Q_{jl}$ are the voltage and current magnitudes, active, and reactive power changes of the j DER terminals after the l load event. σ_{jl} is the wind speed standard deviation measurement at j during each l event.

Although the share of IBR impacts the DS response to dynamic events [10], DSOs are unaware of the specific DS IBR types in operation. Thus, in the proposed coordination, the DSO applies the IBR classifier in Alg. 1 using Ω^{DB} to classify each IBR as GFM or GFL, resulting in the sets Ω^{GFM} and Ω^{GFL}, respectively. The proposed approach assumes that the DSOs know which DERs are synchronous machines, Ω^{SM}, e.g., gas turbines. This assumption differs from alternative approaches that assume known IBR types and DER parameters [25,27].

Algorithm 1 Classifying IBR types

Input: $\Omega^{DB}, \Omega^{DER}, \Omega^{SM}$
Output: $\Omega^{GFM}, \Omega^{GFL}$
1: $\Omega^{GFM} \leftarrow \emptyset, \Omega^{GFL} \leftarrow \emptyset$
2: **for** $j \in \Omega^{DER} \setminus \Omega^{SM}$ **do**
3: $\psi \leftarrow 0$
4: **for** $(\Delta P_{jl}, \sigma_{jl}) \in \Omega^{DB}$ **do** ▷ from (1)
5: $\psi \leftarrow \psi + \Psi(\Delta P_{jl}, \sigma_{jl})$ ▷ using (2)
6: **end for**
7: **if** $\psi > 0$ **then**
8: $\Omega^{GFM} \leftarrow \Omega^{GFM} \cup \{j\}$
9: **else**
10: $\Omega^{GFL} \leftarrow \Omega^{GFL} \cup \{j\}$
11: **end if**
12: **end for**
13: **return** $\Omega^{GFM}, \Omega^{GFL}$

Following DS disturbances such as load changes, GFM IBRs typically reduce or increase the output power to mitigate the disturbance and maintain stable voltage and frequency [32]. In contrast, GFL IBRs typically continue to inject power following the system voltage and frequency [32]. GFL IBRs, including the ones used in the case studies, can also offer frequency support with droop, with the GFM IBR response typically being stronger [33]. The active power threshold diversifying GFM from GFL responses is $\Delta\hat{P}[\%]$. The classifier takes a weighted assignment $\Psi \in [-1, 1]$ on the IBR type after each event l in line 5 of Alg. 1, as:

$$\Psi(\Delta P_{jl}, \sigma_{jl}) = \begin{cases} tanh(\frac{|\Delta P_{jl}| - \Delta\hat{P}}{\sigma_{jl}}), & \text{if } \sigma_{jl} \neq 0, \\ sign(|\Delta P_{jl}| - \Delta\hat{P}), & \text{otherwise,} \end{cases} \tag{2}$$

where $\Psi > 0$ for GFM type, and $\Psi < 0$ for GFL type. Ψ magnitude is the weight for class assignment confidence. The classifier considers wind speed variability during each event as an uncertainty source. Wind deviations can cause changes in IBR outputs unrelated to the load events. Thus the recorded ΔP_{jl} are:

$$\Delta P_{jl} = \Delta\bar{P}_{jl} + \epsilon(\sigma_{jl})[\%], \tag{3}$$

where $\Delta\bar{P}_{jl}$ is the change caused by the actual inverter type of IBR j responding to event l. $\epsilon(\sigma_{jl})$ is the residual uncertainty caused by the wind variability. Inverters and controllers of wind turbines typically include damping mechanisms to reduce output deviations due to weather conditions [34]. These mechanisms reduce the impact of $\epsilon(\sigma_{jl})$ on ΔP_{jl}. Nevertheless, an event l with low σ_{jl} causes a low $\epsilon(\sigma_{jl})$.

Since Ω^{DB} stores multiple load events, Alg. 1 gets $\phi = |\Omega^{\Phi}|$ samples to classify each IBR as GFM or GFL. The class assignment from each sample has a weight of confidence from (2). Alg. 1 sums the weighted class assignments for each IBR. If the accumulated Ψ from all events is non-negative, then the IBR is classified as GFM in lines 7 – 8 of Alg. 1. Otherwise, the IBR is classified as GFL in lines 9 – 10 of Alg. 1. Let a classification metric with a probability of correct classification $\hat{\rho}_l^{\gamma} \in [0, 1]$ for a single load event l. Given ϕ independent load events, the probability of the correct class being predicted for an IBR for the majority of events is:

$$\hat{\rho}_{\phi}^{\gamma} = \sum_{n=\frac{\phi+1}{2}}^{\phi} \binom{\phi}{n} (\hat{\rho}_l^{\gamma})^n (1 - \hat{\rho}_l^{\gamma})^{\phi-n} \in [0, 1], \tag{4}$$

which is the cumulative distribution function of the binomial distribution.

The DSO uses the $\Omega^{GFM}, \Omega^{GFL}$ outputs from the IBR classifier and the constant flow of real-time measurements from RTI to output vector A of parameters that could impact the DS response to dynamic events:

$$A = [\sum_{\hat{j} \in \Omega^{GFM}} P_{\hat{j}}, \sum_{\hat{j} \in \Omega^{GFM}} Q_{\hat{j}}, \sum_{\hat{j} \in \Omega^{GFL}} P_{\hat{j}}, \sum_{\hat{j} \in \Omega^{GFL}} Q_{\hat{j}}, \sum_{\hat{j} \in \Omega^{SM}} P_{\hat{j}}, \sum_{\hat{j} \in \Omega^{SM}} Q_{\hat{j}},$$
$$P_{\hat{j}} \forall \hat{j} \in \Omega^{GFM}, Q_{\hat{j}} \forall \hat{j} \in \Omega^{GFM}, S_{\hat{j}} \forall \hat{j} \in \Omega^{GFM}]^T. \tag{5}$$

where P is active power, Q is reactive power, and S is apparent power.

ADRR models can address the second challenge of Section 2, where a DSO provides a DS ADRR model that the TSO can deploy to perform dynamic simulations. The proposed ADRR model includes the IBR setpoints as inputs for the TSO to evaluate the flexibility actions' impact on the DS response and to address Section 2's third challenge.

2.2. TSOs selecting IBR setpoints

This section analyzes the GFM IBR setpoint optimizer of Fig. 1, which enables TSOs to select IBR setpoints to minimize instability risks for the post-fault response of interconnected DSs and TSs.

Unlike small load disturbances, large disturbances in TSs, such as line faults, are less frequent but can cause instability and high costs for TSOs [9]. The TSO can use the proposed coordination process to avoid instabilities caused by large disturbances. In Fig. 1, the TSO informs the DSO about the setpoint request for all IBRs and the dynamic event (reason for request). The DSO validates DS constraint-feasibility for the TSO requests using DS state estimation (DSSE). DSSE approaches consider measured nodes and pseudo-measured nodal power injections to estimate the DS state [35]. If the requested state respects the DS constraints, the DSO forwards the requests to the GFM IBRs through RTI. Alternatively, the DSO informs the TSO that the setpoints are invalid, so the TSO can explore alternative risk-mitigation sources from neighboring DSOs or TS-connected resources.

The current saturation issue of droop-controlled GFM inverters causes instability if the active power output of the inverter exceeds the limit, as analyzed in [12]. In the proposed approach, TSOs can simulate disturbances in TS with ADRR representing the DS, considering the potential increase in GFM IBR active power after probable disturbances. If these simulations indicate that an increase in the active power output of GFM IBRs would cause instability due to current saturation, reducing the GFM IBR setpoints could result in greater headroom, avoiding reaching maximum current. The proposed approach compares the risks associated with the probability of disturbance and the costs of instability to avoid unnecessary setpoint reductions.

The proposed approach does not depend only on current saturation instabilities. If the DS data for the ADRR model include other sources of post-disturbance instability, the proposed approach can enable TSOs to simulate these responses and evaluate whether reducing the GFM IBR active power can prevent these instabilities.

A large disturbance event e has a probability of occurrence $\hat{\rho}^o(e) \in [0,1]$. If event e causes instability, the potential costs for the TSO can be $C^l(e)$ [€], caused by loss of load in the area or outage costs [9]. Alternatively, the costs of adjusting the GFM IBR setpoints to prevent instability can be $C^\eta(e)$[€/%]. The active power setpoint for all GFM IBRs is P^s[%]. The $\hat{\rho}^l(e,\zeta,A,P^s) \in [0,1]$ is the probability of instability for TS operating condition ζ, and DS attributes of vector A, after e, if P^s is applied. $\hat{\rho}^l(e,\zeta,A,P^s)$ is independent of $\hat{\rho}^o(e)$. Thus, the risk for the TSO, $R(e,\zeta,A,P^s)$, for e is:

$$R(e,\zeta,A,P^s) = \hat{\rho}^o(e)\cdot\bar{R}(e,\zeta,A,P^s) + (1-\hat{\rho}^o(e))\cdot C^\eta(e)\cdot(100-P^s)[€], \tag{6}$$

$$\bar{R}(e,\zeta,A,P^s) = C^l(e)\cdot\hat{\rho}^l(e,\zeta,A,P^s) + C^\eta(e)\cdot(100-P^s)[€]. \tag{7}$$

where $\bar{R}(e,\zeta,A,P^s)$ is the risk for the TSO if e occurs. Thus combining (6) and (7) leads to:

$$R(e,\zeta,A,P^s) = \hat{\rho}^o(e)\cdot C^l(e)\cdot\hat{\rho}^l(e,\zeta,A,P^s) + C^\eta(e)\cdot(100-P^s)[€]. \tag{8}$$

Let $\overline{P^s}$[%], the maximum setpoint for all GFM IBRs addressing the potential instability event. TSOs can either neglect the potential impact of e or apply $\overline{P^s}$ by assessing the risks of these actions as:

$$P^{s*} = \underset{P^s\in\{\overline{P^s},100\}}{\operatorname{argmin}} \Big(R(e,\zeta,A,P^s)\Big)[\%], \tag{9}$$

where P^{s*}[%] is the minimum-risk setpoint.

The GFM IBR active power setpoint optimizer of Fig. 1 and Alg. 2 identifies the minimum-risk setpoint P^{s*}, of resolution δP[%], for GFM IBRs to avoid the potential instability from the large disturbance e. The optimizer first identifies the maximum feasible setpoint $\overline{P^s}$ and then applies (9) to obtain P^{s*}. To estimate $\overline{P^s}$, Alg. 2 performs a tree search for a list of setpoint levels Γ^s. The inputs $\bar{\Lambda}$ are the TSO stability thresholds, i.e., limits for frequency, voltage, rate of change of frequency (RoCoF), and active and reactive power deviations. Λ are the simulated values for the above thresholds. P^s_{min}[%] is the minimum setpoint evaluated by the algorithm. $\tilde{A}$ is the value for A if P^s is applied. The function $F^s(A,P^s)$ applies the selected setpoints P^s to the GFM IBR attributes of A, representing controlling the GFM IBR setpoints on line 6 of Alg. 2. $F^{sim}(e,\zeta,A)$ performs the dynamic simulation considering e and the DS and TS operating condition on line 7 of Alg. 2. If no setpoint can solve the instability, the $\overline{P^s} = 100$ from line 3 of Alg. 2 shows that none of the changes provided a solution, thus (9) returns no action on line 25 of Alg. 2. The setpoint optimizer does not intend to control the voltage or frequency post-fault response to specific follow trajectories, but rather reduce the risks for post-fault instability, considering the ADRR and TS simulated responses.

In the proposed coordination, TSOs can identify potential communication failures by detecting disruptions in the information flow between RTI measurements and vector A input for the DS ADRR, as in Fig. 1. In such cases, TSOs should use previously measured vector A instances until communication is restored. If simulations indicate instability, TSOs should only consider instability preventive measures outside the DS controllable devices until RTI communications are re-established.

Algorithm 2 GFM IBR Active Power Setpoint Optimizer

Input: $e,\zeta,A,\delta P,\bar{\Lambda},P^s_{min},\hat{\rho}^o(e)$
Output: P^{s*}

1: $\Gamma^s \leftarrow [P^s_{min}, P^s_{min}+\delta P, P^s_{min}+2\delta P, .., 100]$
2: $P^s_{max} \leftarrow 100$
3: $\overline{P^s} \leftarrow 100$
4: **while** $\Gamma^s != [\ ]$ **do**
5: $\quad P^s \leftarrow \Gamma^s[\lfloor \frac{\text{length}(\Gamma^s)}{2} \rfloor]$ ▷ Get the median value
6: $\quad \tilde{A} \leftarrow F^s(A,P^s)$
7: $\quad \Lambda \leftarrow F^{sim}(e,\zeta,\tilde{A})$
8: $\quad$ **if** $\Lambda <= \bar{\Lambda}$ **then**
9: $\quad\quad$ **if** $P^s+\delta P < P^s_{max}$ **then**
10: $\quad\quad\quad \Gamma^s \leftarrow [P^s+\delta P, .., P^s_{max}]$
11: $\quad\quad$ **else**
12: $\quad\quad\quad \Gamma^s \leftarrow [\ ]$
13: $\quad\quad$ **end if**
14: $\quad\quad \overline{P^s} \leftarrow P^s$
15: $\quad\quad P^s_{min} \leftarrow P^s$
16: $\quad$ **else**
17: $\quad\quad$ **if** $P^s_{min} < P^s - \delta P$ **then**
18: $\quad\quad\quad \Gamma^s \leftarrow [P^s_{min}, P^s_{min}+\delta P, .., P^s-\delta P]$
19: $\quad\quad$ **else**
20: $\quad\quad\quad \Gamma^s \leftarrow [\ ]$
21: $\quad\quad$ **end if**
22: $\quad\quad P^s_{max} \leftarrow P^s$
23: $\quad$ **end if**
24: **end while**
25: $P^{s*} \leftarrow$ (9) with $e,\zeta,A,\overline{P^s}$
26: **return** P^{s*}

3. Aggregated dynamic response representation

This section describes the methodology in the proposed DS ADRR model. This methodology includes the reasoning for the selected learning architectures and their structure. The proposed DS ADRR model, as shown in Fig. 1, enables the TSO to simulate the post-fault response of the DS considering the setpoints for DS IBRs. The proposed coordination of Fig. 1 uses the IBR Classifier and vector A from (5) to inform the DS ADRR model on the DS condition. The setpoint optimizer of

Section 2.2 allows the TSO to optimize and evaluate GFM IBR setpoints using the DS ADRR model.

The proposed ADRR model includes a regressor representing the DS response to a large TS disturbance in a simulation and a classifier to detect high instabilities and terminate the simulation process. Power systems simulation software, such as PowerFactory rely on iterative numerical methods. Highly instable conditions can cause no results or non-convergence issues in the numerical methods. These issues can further delay the simulations, lead to possibly erroneous results, or terminate the simulations early. Extreme spikes caused by these instable conditions can dominate optimization losses and reduce the overall ADRR model accuracy. The proposed ADRR structure identifies these highly instable conditions to inform TSOs about the high instability. The following two subsections describe this regressor and classifier of the ADRR model.

3.1. ADRR regression model

Existing ADRR approaches typically do not require non-sequential features or do not use RNNs that focus on sequential features. Sequential features $x(t)$ are essential to capture the temporal dependencies of dynamic simulations. The non-sequential features z, which include vector A from (5), provide information on the initial DS operating condition and DS sensitivity to the IBR outputs. Sequential features depend on the dynamic simulation time-step t, e.g., total DS active power output $P(t)$. The simulation time-step does not impact non-sequential features, e.g., initial DS active power output. RNN architectures such as LSTMs and gated recurrent units have gated mechanisms to keep long- and short-term dependencies in the sequential variables. To capture temporal dependencies, a feedforward neural network (FNN) would require input vectorized sequences of variables that can be less effective than RNNs.

The proposed model of Fig. 2 uses the RNN specialization for sequential features $x(t)$ and applies a linear dense layer on non-sequential features z. The sequential input feature matrix $x(t)$ includes the PCCs' voltage magnitudes $v(t)$ and angles $\theta(t)$, the frequency $f(t)$ and their previous values in a window μ as:

$$x(t) = [\hat{x}(t), \hat{x}(t-\tau), .., \hat{x}(t-\mu\cdot\tau)], \tag{10}$$

$$\hat{x}(t) = [v_{PCC_1}, v_{PCC_2}, \theta_{PCC_1}, \theta_{PCC_2}, f]^T(t), \tag{11}$$

where $\tau[s]$ is the simulation time-step, and PCC_1, PCC_2 are the 2 PCCs in ring DS topologies. The non-sequential inputs are the PCCs' initial power outputs P^0_{PCC}, Q^0_{PCC}, the TS inertia characteristic constant H, and the features vector A from (5):

$$z = [P^0_{PCC_1}, P^0_{PCC_2}, Q^0_{PCC_1}, Q^0_{PCC_2}, H, A^T]^T. \tag{12}$$

As Fig. 2 shows, the proposed model performs feature fusion, concatenating the dense and RNN layer outputs. A FNN uses the combined outputs to predict the DS response.

The vector of observed active and reactive power at each PCC at each time step t is:

$$y(t) = [P_{PCC_1}, P_{PCC_2}, Q_{PCC_1}, Q_{PCC_2}]^T(t). \tag{13}$$

For a single-PCC DS, y would exclude the features and outputs for PCC_2. For DSs with more PCCs, y would expand the features and outputs for each additional PCC, e.g., v_{PCC3}.

The function describing the proposed model of Fig. 2 is:

$$\hat{y}(t) = F^{FN}_{w_{FN}}\left(F^{FF}(\hat{y}_x(t), \hat{y}_z)\right). \tag{14}$$

where $\hat{y}_x(t)$ is the output of the RNN layers and $\hat{y}_z$ is the output of the dense layer. F^{FF} is the feature fusion function, concatenating the RNN and FNN model outputs. $F^{FN}_{w_{FN}}$ is the FNN model that takes the fused features as inputs, and outputs the $\hat{y}(t) \in \mathrm{R}^4$; to approximate the observed $y(t)$. The w_{FN} are the learnable weights of the FNN model.

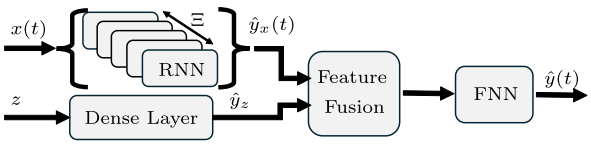

Fig. 2. Proposed ADRR regression model.

The proposed RNN, as in [19], deploys Ξ LSTM RNNs in parallel with their outputs being concatenated in vector $\hat{y}_x(t)$ as:

$$\hat{y}_x(t) = [\hat{y}_{RNN_0}, .., \hat{y}_{RNN_\Xi}]^T(t), \tag{15}$$

$$\hat{y}_{RNN_\xi}(t) = F^{RNN}_{w_\xi}(x(t), \hat{y}_{RNN_\xi}(t-1)) \forall \xi \in [0, \Xi], \tag{16}$$

where $F^{RNN}_{w_\xi}$ is the ξ^{th} RNN model and w_ξ the learnable weights. The dense layer output is:

$$\hat{y}_z = F^{DL}_{w_z}(z), \tag{17}$$

where $F^{DL}_{w_z}$ is the dense layer and w_z the learnable weights.

The regression objective is to find parameters $w = \{w_{FN}, w_\xi \forall \xi \in \Xi, w_z\}$ to minimize the error between the model outputs and observed DS outputs. Hence, the loss function L is the root mean squared error (RMSE) between y and $\hat{y}$ as:

$$L = \frac{1}{|D|\cdot\kappa}\sqrt{\sum_{d\in D}\sum_{k=0}^{k=\kappa}(y(k\cdot\tau) - \hat{y}(k\cdot\tau))^2}, \tag{18}$$

where $|D|$ is the length of dataset D with samples $d = (x(0), .., x(\kappa\cdot\tau), y(0), .., y(\kappa\cdot\tau), z) \in D$. κ is the number of time steps for each simulation.

3.2. Classification of instabilities

High instabilities can be present in simulations with low TS inertia. ADRR models could inform TSOs and help them avoid these high instabilities. Unlike related literature, the proposed ADRR model also includes a classifier for high instabilities during the simulation to inform the TSO. Excluding the high instability classifier means including simulations with extreme values and fluctuations that could dominate the regression model's loss and learning process.

Classifying extreme instabilities requires analyzing sequential data to detect high fluctuations. However, assigning all sequence values as unique features in an FNN can be inefficient. The most prominent methods for time-series classification first process each signal to get low dimensional features and apply ML-based techniques to classify using these low dimensional features [36]. The proposed approach applies feature-based (FB) time series classification [36].

The classifier first gets the input χ that includes the simulation results between the 0.5 [s] before, and 1.5 [s] after the disturbance as:

$$\chi = \begin{bmatrix}\hat{x}(t_e - 0.5), \hat{x}(t_e - 0.5 + \tau), .., \hat{x}(t_e + 1.5)\\ \hat{y}(t_e - 0.5), \hat{y}(t_e - 0.5 + \tau), .., \hat{y}(t_e + 1.5)\end{bmatrix}, \tag{19}$$

where $t_e[s]$ is the event time. Since the proposed coordination uses ADRR to simulate potential events as in Fig. 1, t_e is an input to the simulation. Considering typically small τ in dynamic simulations, χ can be high-dimensional. The proposed approach applies the feature extractor function F^{FE} to analyze the time series of each signal in χ and get a low-dimensional vector π as:

$$\pi = F^{FE}(\chi). \tag{20}$$

The F^{FE} estimates correlation coefficients across all signals. For each signal, F^{FE} estimates the variance, discrete Fourier transform coefficients, the mean power of frequency bands from the signal power spectrum, and the number of peaks in the signal. The classifier FNN

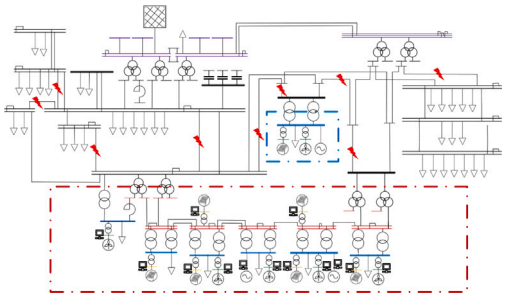

Fig. 3. Test system diagram, with the DS, external grid, neighboring DS, loads, PV modules, wind turbines, synchronous machines, RTI measurement locations. The indicate the simulated fault event locations.

uses the π feature vector and labels the output as highly instable or not:

$$\hat{y}_\chi = F^{CL}_{w_\chi}(\pi) \in \{0, 1\}, \tag{21}$$

where $F^{CL}_{w_\chi}, w_\chi$ are the FNN classifier and its weights.

4. Case studies

The case studies showcase the proposed coordination's components in selecting IBR setpoints to minimize post-fault instability risks, providing ADRR, and classifying highly instable conditions.

4.1. Test system and synthetic data generation

The system used includes the synthetic TS and DS models of the Zeeland province in the Netherlands, shown in Fig. 3. The diagram includes the DS of which the ADRR model is developed (surrounded by red dashed lines), the TS, the DER of a second DS (surrounded by blue dashed lines), and the external grid for the rest of the TS. The TS has 150 [kV] and 380 [kV] buses. The DS has 52.5 [kV] and 10.6 [kV] buses. The model is in DigSilent Powerfactory. TSO TenneT provided the TS and [37] the DSs. The DSs were modified to include the 2024 DER capacity and load consumptions. The DS line and transformer capacity were increased by 4 times from [37] to accommodate the increased DER capacity. The system includes GFM IBRs (Droop Control System), GFL IBRs (WECC WT Control System Type 4A), and synchronous machines.

The ADRR model dataset includes 1545 fault-event simulations (faulted lines were randomly sampled from the 9 options in Fig. 3). The supplementary material includes details on data generation.

4.1.1. Case study settings

The case study of Section 4.3 compares the proposed ADRR model to baselines:

(i) An FNN as [26], showcasing the impact of excluding LSTM in ADRR. This model includes the ADRR classifier.

(ii) An LSTM including sequential and repeated non-sequential input features followed by an FNN, showcasing the impact of excluding feature fusion and dense layer for non-sequential features in ADRR. This model is a natural extension of [19,38] to include non-sequential features. This model includes the ADRR classifier.

(iii) The proposed structure, excluding the ADRR classifier. This model studies the impact of including extreme values observed in highly instable samples in ADRR.

(iv) An LSTM followed by an FNN, excluding non-sequential features, such as [19,38]. This model studies the impact of excluding non-sequential features in ADRR.

The model comparison metric was the RMSE on a test set of simulated events. Section 4.4 case study analyzes the proposed ADRR classifier and compares it with baselines:

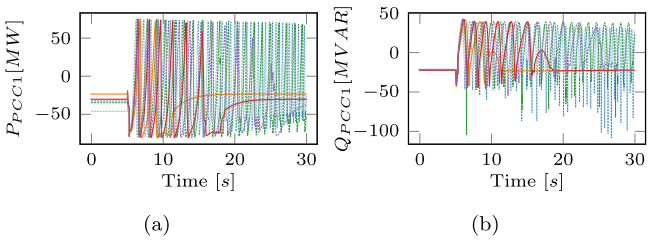

Fig. 4. The response of the DS at PCC 1 after the same fault with setpoints of $P^s = 100[\%]$ (), $P^s = 50[\%]$ (), $P^s = 75[\%]$ (), $\overline{P^s} = 65[\%]$ (), and $P^s = 70[\%]$ ().

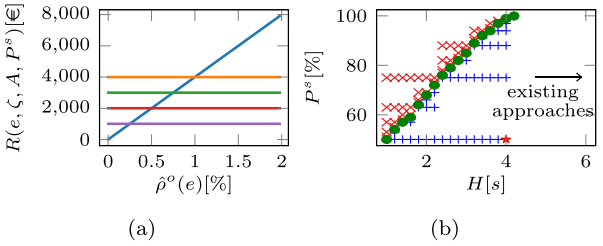

Fig. 5. In (a), example risks for different fault event probabilities. Risks without reduction (), or with reduction if $\overline{P^s} = 60[\%]$ (), if $\overline{P^s} = 70[\%]$ (), if $\overline{P^s} = 80[\%]$ (), or if $\overline{P^s} = 90[\%]$ (). In (b), the setpoint optimizer's search for maximum feasible $\overline{P^s}[\%]$ with $\delta P = 1[\%]$ for different levels of $H[s]$. Feasible (+), not-feasible (×, ★), and $\overline{P^s}$ ().

1. A classifier with additional features, the 5 coefficients when fitting the signal with the autoregressive moving-average (ARMA) model [39]. ARMA features are commonly used for FB time series classification as dynamic features [36].
2. A distance-based (DB) classifier [36], using dynamic time warping to estimate the distance between the signals as a similarity score. Using this similarity score, a k-nearest neighbors classifier predicted if each test sample was highly instable.

The precision metric is the ratio of correctly classified samples as highly instable to all samples classified as highly instable. The recall metric is the ratio of samples correctly classified as highly instable to all highly instable samples. The accuracy metric is the ratio of correct predictions to all predictions. Supplementary material includes details on model structure and training, and additional case studies.

4.2. GFM IBR active power setpoint optimizer

This case study investigates the setpoint optimizer of Alg. 2 in Section 2.2. The setpoint optimizer simulates the DS response under different reduced GFM outputs to identify the maximum feasible setpoint and evaluate the risk of applying the setpoint. Fig. 4 shows the simulated responses of different GFM setpoints. When reduced to 65[%] or 50[%], the post-disturbance DS response did not breach the stability constraints for $RoCoF$, under/over frequency, or under/over voltage. Thus, $\overline{P^s} = 65[\%]$. Without any action, $C^l(e) \approx 400k[€]$, whereas applying (9) would suggest requesting $\overline{P^s} = 65[\%]$ if $\hat{\rho}^o(e) \geq 0.9[\%]$. Deterministically controlling the setpoints whenever instability can happen ($\hat{\rho}^o(e) = 100[\%]$), could for example require applying $\overline{P^s} = 65[\%]$, 40 times per year, resulting in $\approx 280k[€]$. Probabilistically applying (9) only when $\hat{\rho}^o(e) > 0.9[\%]$ (e.g. 20 times per year) would result in $\approx 140k[€]$.

Fig. 5 shows how a low TS H requires a larger reduction in GFM IBR active power to avoid saturation after the disturbance. In TSs with low inertia, disturbances lead to larger frequency deviations and more volatile dynamic responses. GFM IBRs, which aim to regulate frequency and voltage through active and reactive power injection, can

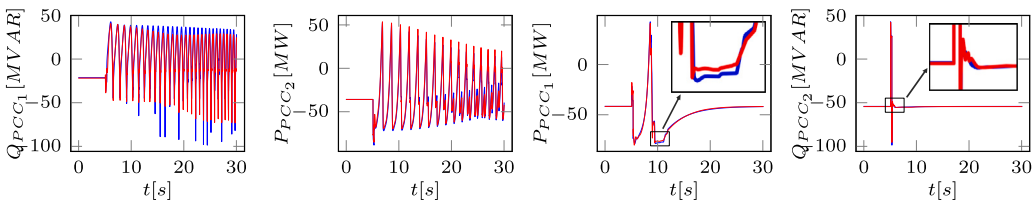

(a) RMSE=8.01[$MVAR$]. (b) RMSE=4.66[MW]. (c) RMSE 2.29[MW]. (d) RMSE 0.27[$MVAR$].

Fig. 6. Example RMSE levels from model predictions (▬), compared to the simulated signals (▬).

Table 1
Proposed model baseline model performances.

Model	Training RMSE	Validation RMSE	Test RMSE	Training [h]
Proposed	0.83	0.98	0.94	8
(i)	1.06	1.29	1.29	7
(ii)	3.98	4.26	3.61	18
(iii)	2.96	3.2	3.03	8
(iv)	2.21	2.39	2.32	8

face higher demands after these disturbances. These demands can push the GFM IBRs to their current saturation limits. Upon reaching these limits, GFM IBRs can lose synchronous stability [12].

At $H = 4$ [s], a low setpoint value of 50[%] let to instable conditions. Therefore, for higher inertia $H \geq 3.5$ [s], setting $P^s_{min} \geq 25$[%] can avoid such issues and reduce the iterations of Alg. 2. As TS H increases, the post-fault frequency deviations are less volatile. Therefore, GFM IBRs require lower active power changes to address frequency deviations. Existing ADRR approaches represent TS with high inertia. Thus, in existing approaches, IBRs do not apply significant power output adjustments to control the system frequency and voltage, and do not reach their saturation current. The computational burden for Fig. 5(b) was between 20 s and 6 min. Considering preventive coordination, this burden is not restrictive for TSOs.

4.3. ADRR regression model

This case study compares the proposed ADRR regression model of Section 3.1 to the baselines through the RMSE metric for predictions of the ADRR test set. Fig. 6 shows example model predictions and RMSEs. Table 1 compares the proposed model to baseline ADRR models. Table 1 shows the proposed structure outperforms the fine-tuned baselines. Model (i) shows a higher mismatch between training and test errors, indicating a potential for overfitting compared to the other models.

The training duration for model (ii) was more substantial than the rest, as the number of non-sequential features is larger than the sequential, and replicating their values is inefficient. All model training times allow frequent (e.g., monthly) re-training intervals.

The proposed ADRR model structure of Fig. 2 outperforms the baseline structures. The model (i) structure is as [26], model (iv) structure is as [19,38], whereas model (iii) is as [19,38] extended to include non-sequential features in the LSTM inputs. Models (i), (ii), (iv), unlike [19, 26,38], also include the classifier as it improves the RMSE, as shown by model (iii) performance compared to the proposed model. Comparing the proposed model with model (i), including RNNs is important for sequential features. Replicating and considering the non-sequential features as sequential is inefficient and can deteriorate the performance, as in model (ii). This result is expected as the non-sequential features outnumber the sequential. Removing the non-sequential features also deteriorates the performance, as in model (iv). Excluding the ADRR classifier for high instabilities burdens the regression model with high value and fluctuation prediction, deteriorating the model performance as with model (iii).

This case study also estimated the DS response using the proposed ADRR model for the setpoint optimizer task of Fig. 4. Fig. 7 shows the

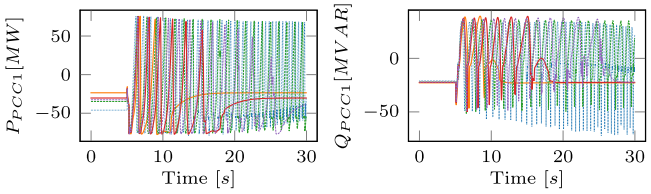

(a) (b)

Fig. 7. The response of the ADRR model at PCC 1 after the same fault with setpoints of P^s = 100[%] (·····), P^s = 50[%] (▬), P^s = 75[%] (- - - -), P^s = 65[%] (▬), and P^s = 70[%] (- - -).

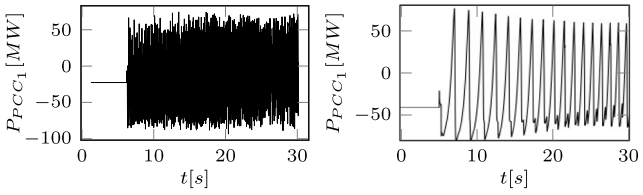

(a) Highly Instable Simulation. (b) Regressor Instable Simulation.

Fig. 8. Example samples classified as highly instable (a) and not (b).

ADRR model response led to the exact conclusions as the simulated DS response. These conclusions were the maximum feasible setpoint of 65[%], with 50[%] being feasible, and 70, 75, 100[%] non-feasible. The ADRR outputs of Fig. 7 approximate the simulations of Fig. 4.

4.4. High instability classification

This case study investigates the high instability classifier of Section 3.2. Fig. 8 shows examples of highly instable and regressor samples. Table 2 compares the performance of the proposed FB model, the baseline FB model with added ARMA features, and the DB model. The prediction time indicates the delay each ADRR classifier adds to the ADRR, including the sample feature extraction. This classification delay only happens once per simulated event. Including the ARMA features does not improve the model accuracy, precision, or recall, but highly delays the prediction and feature extraction processes. The delay the proposed FB model adds once for each dynamic simulation (0.3 [s]) is minor. The FB models outperform the DB in accuracy and recall. The 100[%] precision indicates that all models correctly identified all non-highly-instable simulations in the test set. The proposed high instability classifier shows the highest accuracy with the lowest delays among the options.

4.5. Discussion

Considering the challenges for TSOs assessing the IBR flexibility for dynamic events, the case studies show the applicability of the proposed coordination. The ADRR model represents the post-disturbance DS

Table 2
Classification model performances.

Model	FB	FB with ARMA	DB
Test accuracy [%]	99.7	99.7	99
Test precision [%]	100	100	100
Test recall [%]	98.0	98.0	94.1
Feature extraction and training [min]	0.63	110	0.11
Prediction [s]	0.3	4.7	0.57

response. The GFM IBR active power setpoint optimizer can use the ADRR model's GFM IBR setpoint inputs to reduce instability risks. The identified setpoints when using the proposed ADRR model are similar to the simulations with the DS. Insights from the simulated responses are:

1. The system can withstand faults without reducing the GFM IBR setpoints when the TS inertia is high.
2. GFM IBRs require a headroom to avoid reaching their saturation current when the TS inertia is low.
3. The GFM IBR maximum feasible setpoint increases as the TS inertia increases.
4. Reducing the GFM IBR setpoints multiple times to prevent instabilities can cost less than suffering outages due to instabilities.
5. Probabilistically reducing the setpoints, considering instability risks, reduces the costs of preventing instability.

This research offers a coordination process that limits the instability risks from IBRs' current saturation issues. In the proposed coordination, TSOs inform DSOs and IBRs about the reason for the requested setpoint, as RTI requires.

The proposed IBR classifier considers a stronger response of GFM IBRs in the presence of droop-controlled GFL IBRs. With increased diversity and complexity in GFM and GFL IBR modes, the IBR classifier should include a more complex algorithm and possibly consider additional data sources to classify the IBR modes. The test set included scenarios unseen during ADRR training, which varied in operating conditions, TS inertia, fault locations, and fault durations. The proposed ADRR results indicated a low RMSE for this test set and variability of scenarios. However, topological or structural changes in DSs can challenge data-driven ADRR models. Therefore, for structural and topological changes, additional data generation and ADRR model retraining or calibration are needed. A further limitation, the proposed approach did not co-simulate the ADRR model and transmission network, due to the absence of ML-based models in PowerFactory dynamic simulations. Therefore, DSOs and TSOs can adopt the proposed coordination when dynamic simulation software accepts ML-based models.

5. Conclusion

The proposed TSO-DSO coordination method allows TSOs to simulate the DS response to potential faults, evaluate the impact of different GFM IBR setpoints, and control these setpoints to prevent instabilities. This application addresses one of the key challenges recognized by the European DSO Entity and ENTSO-E [40]; the system's resilience through shared risk assessment, which requires risk assessment models, data-sharing, and coordination across stakeholders. The coordination uses RTI to classify the IBR types, identify the DS condition, and control the IBR setpoints. The proposed ADRR approach accounts for the transmission system's dynamic properties and share of IBR types that impact the DS response to dynamic events. The proposed ADRR model also allows TSOs to modify DS GFM IBR setpoints and analyze their impact. The proposed risk-based evaluation and setpoint selection can identify the TSO's minimum-risk setpoints.

In the Netherlands, the IBR response to dynamic events can impact the stability in TS with low inertia (e.g., below 4 [s]). Thus, controlling the IBR setpoints under low-inertia TSs reduces instability risks, considering the probability of a dynamic event. Including the TS dynamic properties, DS operating condition, and IBR share improves the prediction performance by 59[%] (RMSE reduced from 2.32 to 0.94).

Future work includes exploring flexibility areas in the proposed coordination process to inform TSOs on the potential feasibility of the IBR control setpoints on the DS steady-state constraints. Subsequent work will also consider alternative test systems and IBR models to explore the proposed approach's performance under alternative sources of instability. The adaptability of ADRR models to different topologies will also be studied. Future developments will explore developing a computationally feasible algorithm to optimize different individual setpoints per GFM IBR. Next steps also include designing an IBR classifier that adaptively screens and differentiates the dynamic response of GFM and GFL IBRs.

CRediT authorship contribution statement

Demetris Chrysostomou: Writing – review & editing, Writing – original draft, Visualization, Validation, Software, Methodology, Investigation, Formal analysis, Data curation, Conceptualization. **José Luis Rueda Torres:** Writing – review & editing, Writing – original draft, Validation, Supervision, Project administration, Methodology, Conceptualization. **Jochen Lorenz Cremer:** Writing – review & editing, Writing – original draft, Validation, Supervision, Project administration, Methodology, Conceptualization.

Declaration of competing interest

The authors declare that they have no known competing financial interests or personal relationships that could have appeared to influence the work reported in this paper.

Acknowledgments

This research is part of the research program 'MegaMind - Measuring, Gathering, Mining and Integrating Data for Self-management in the Edge of the Electricity System', (partly) financed by the Dutch Research Council (NWO) through the Perspectief program under number P19-25.

The Dutch TSO, TenneT, provided the transmission system model used in the case studies.

Appendix A. Supplementary data

Supplementary material related to this article can be found online at https://doi.org/10.1016/j.ijepes.2025.111353.

Data availability

The data that has been used is confidential.

References

[1] Chaspierre G, Denis G, Panciatici P, Van Cutsem T. An active distribution network equivalent derived from large-disturbance simulations with uncertainty. IEEE Trans Smart Grid 2020;11(6).
[2] Givisiez AG, Petrou K, Ochoa LF. A review on TSO-DSO coordination models and solution techniques. Electr Power Syst Res 2020.
[3] Vicente-Pastor A, Nieto-Martin J, Bunn DW, Laur A. Evaluation of flexibility markets for retailer–DSO–TSO coordination. IEEE Trans Power Syst 2018;34(3).
[4] Vagropoulos SI, Biskas PN, Bakirtzis AG. Market-based TSO-DSO coordination for enhanced flexibility services provision. Electr Power Syst Res 2022;208.
[5] Troncia M, Chaves Ávila JP, Damas Silva C, Gerard H, Willeghems G. Market-based TSO–DSO coordination: A comprehensive theoretical market framework and lessons from real-world implementations. Energies 2023;16(19):6939.
[6] Chrysostomou D, Rueda Torres JL, Cremer JL. Exploring operational flexibility of active distribution networks with low observability. In: IEEE belgrade powerTech. 2023.
[7] Chrysostomou D, Torres JLR, Cremer JL. Tensor convolution-based aggregated flexibility estimation in active distribution systems. IEEE Trans Smart Grid 2024.

[8] Cremer JL, Strbac G. A machine-learning based probabilistic perspective on dynamic security assessment. Int J Electr Power Energy Syst 2021;128.
[9] Kundur P, Paserba J, Ajjarapu V, et al. Definition and classification of power system stability IEEE/CIGRE joint task force on stability terms and definitions. IEEE Trans Power Syst 2004;19(3).
[10] Quedan A, Wang W, Ramasubramanian D, Farantatos E, Asgarpoor S. Behavior of a high inverter-based resources distribution network with different participation ratios of grid-forming and grid-following inverters. In: North American power symposium. NAPS, IEEE; 2021.
[11] Pattabiraman D, Lasseter. RH, Jahns TM. Comparison of grid following and grid forming control for a high inverter penetration power system. In: IEEE power & energy society general meeting. 2018.
[12] Xin H, Huang L, Zhang L, Wang Z, Hu J. Synchronous instability mechanism of P-f droop-controlled voltage source converter caused by current saturation. IEEE Trans Power Syst 2016;31(6).
[13] Alshahrani S, Khan K, Abido M, Khalid M. Grid-forming converter and stability aspects of renewable-based low-inertia power networks: Modern trends and challenges. Arab J Sci Eng 2024.
[14] Makolo P, Zamora R, Lie T-T. The role of inertia for grid flexibility under high penetration of variable renewables - a review of challenges and solutions. Renew Sustain Energy Rev 2021;147.
[15] ENTSO-E. Inertia and rate of change of frequency (RoCoF). 2020, URL https://www.fingrid.fi/en/electricity-market-information/.
[16] Laasonen M. Inertia of the Nordic power system, URL https://www.fingrid.fi/en/electricity-market-information/InertiaofNordicpowersystem/.
[17] Dalhues S, Zhou Y, Pohl O, et al. Research and practice of flexibility in distribution systems: A review. CSEE J Power Energy Syst 2019;5(3).
[18] Milanovic JV, Zali SM. Validation of equivalent dynamic model of active distribution network cell. IEEE Trans Power Syst 2012.
[19] Zheng C, Wang S, Liu Y, Liu C, et al. A novel equivalent model of active distribution networks based on LSTM. IEEE Trans Neural Netw Learn Syst 2019;30(9).
[20] Mitrentsis G, Lens H. A Gaussian process framework for the probabilistic dynamic modeling of active distribution networks using exogenous variables. Electr Power Syst Res 2022;211.
[21] Shang X, Li Z, Zheng J, et al. Equivalent modeling of active distribution network considering the spatial uncertainty of renewable energy resources. Int J Electr Power Energy Syst 2019.
[22] Wang P, Zhang Z, Huang Q, Tang X, Lee W-J. Robustness-improved method for measurement-based equivalent modeling of active distribution network. IEEE Trans Ind Appl 2021;57(3).
[23] Kontis EO, Papadopoulos TA, Syed MH, et al. Artificial-intelligence method for the derivation of generic aggregated dynamic equivalent models. IEEE Trans Power Syst 2019.
[24] Kontis EO, del Nozal AR, Dimoulias SC, et al. Dynamic equivalent model of active distribution networks providing frequency-related ancillary services to the transmission system. Appl Energy 2024.
[25] Ungerland J, Poshiya N, Biener W, Lens H. A voltage sensitivity based equivalent for active distribution networks containing grid forming converters. IEEE Trans Smart Grid 2022;14(4).
[26] Azmy AM, Erlich I, Sowa P. Artificial neural network-based dynamic equivalents for distribution systems containing active sources. IEE Proc, Gener Transm Distrib 2004;151(6).
[27] Barać B, Krpan M, Capuder T. Aggregated model of a flexible multi-energy distribution system for coordinated TSO-DSO fast frequency services provision. In: International conference on smart energy systems and technologies. SEST, 2023.
[28] Chychykina I, Styczynski ZA, Heyde CO, Krebs R. Power system instability prevention and remedial measures with online dynamic security assessment. In: 2015 IEEE eindhoven powerTech. 2015.
[29] Liu T, Liu Y, Liu J, et al. A Bayesian learning based scheme for online dynamic security assessment and preventive control. IEEE Trans Power Syst 2020;35(5).
[30] WG TS. Realtime Interface System Operator - DER Dutch implementation of RfG interface requirements Technical Specification Document. Tech. rep., Netbeheer Nederland; 2024.
[31] Primadianto A, Lu C-N. A review on distribution system state estimation. IEEE Trans Power Syst 2017;32(5).
[32] Bevrani H, Kato T, Ise T, Inoue K. Grid Connected Converters: Modeling, Stability and Control. Elsevier; 2022.
[33] Matevosyan J, Badrzadeh B, Prevost T, Quitmann E, Ramasubramanian D, Urdal H, Achilles S, MacDowell J, Huang S, Vital V, OSullivan J, Quint R. Grid-forming inverters: Are they the key for high renewable penetration? IEEE Power Energy Mag 2019;17.
[34] Rezai L, Poschke F, Andrejewski M, Schulte H, Fortmann J. Evaluating flicker damping capabilities of wind turbine inverters with grid following and grid forming controls applying the proposed IEC 61400-21-4. In: 21st wind & solar integration workshop. IET; 2022.
[35] Habib B, Isufi E, van Breda W, Jongepier A, Cremer JL. Deep statistical solver for distribution system state estimation. IEEE Trans Power Syst 2024;39(2):4039–50.
[36] Susto GA, Cenedese A, Terzi M. Time-series classification methods: Review and applications to power systems data. Big Data Appl Power Syst 2018.
[37] Rietveld G, Jongepier A, van Seters J, Visser M, Liu P, Acanski M, Hoogenboom D, van den Brom H. Application of PMUs for monitoring a 50 kv distribution grid. In: Proceedings of the 23rd international conference on electricity distribution. CIRED, 2015.
[38] Li Y, Guerrero JM, Yang J, Guan Y, Ma G, Feng J. Dynamic equivalent modeling for black-box microgrids under multi-operating-point by using LSTM. CSEE J Power Energy Syst 2022;10(2).
[39] Choi B. ARMA Model Identification. Springer Science & Business Media; 2012.
[40] Report TSO-DSO Challenges & Opportunities for Digital Electricity System. Tech. rep., ENTSO-E; 2025, (Accessed 30 April 2025).